DC Conduction and Breakdown Behavior of Thermally Sprayed Ceramic Coatings

Minna Niittymäki, Kari Lahti
Tampere University of Technology
Department of Electrical Engineering
P.O. Box 692
FI-33101 Tampere, Finland

Tomi Suhonen and **Jarkko Metsäjoki**
VTT Technical Research Centre of Finland
P.O. Box 1000
FI-02044 VTT, Finland

ABSTRACT

In this study, the DC conductivity from low electric fields up to breakdown fields is studied for several different thermally sprayed ceramic coatings. Although the DC conductivity of bulk alumina ceramic has been observed to follow the space charge limited current conduction mechanism, the studied ceramic coatings do not follow or follow only partly this mechanism. Possible reason for this is their different microstructure since bulk alumina exhibits fully crystalline microstructure while the ceramic coating consists of crystalline and amorphous regions as well as voids, defects and numerous interfaces. A possible conduction mechanism of the ceramic coatings based on the different conductivities of the amorphous and crystalline regions of the coatings is proposed. The microstructural features (e.g. volumetric porosity) are found to affect the breakdown strength for some of the studied coatings. The step-test breakdown strengths of the coatings were lower than the ramp-test ones due to the longer stress durations in step tests giving an indication of effects of electrical stress duration and possible short-term degradation of the coatings.

Index Terms — **Dielectric breakdown, conductivity, thermally sprayed ceramic coating, alumina, spinel.**

1 INTRODUCTION

THERMALLY sprayed electrically insulating coatings can be utilized in special operation conditions like in harsh environments or in high temperature applications such as in solid oxide fuel cells where the typical operating temperatures can vary from 500 to 800 °C [1]. Typically, the materials used for manufacturing of insulating coatings are alumina (Al_2O_3) or spinel ($MgAl_2O_4$) which can be either in powder or cord form. In the spraying process, thermal energy is generated either by chemical (combustion) or electrical (plasma or arc) methods in order to melt and accelerate the powder particles towards the substrate [2, 3]. The molten particles form droplets which hit the substrate or coating surface forming a coating consisting of thin layers of lamellae (called splats) with interfaces in between [2, 3]. The surfaces of the splats cool down faster than the internal parts and due to this the surfaces are normally more amorphous, while the internal parts are typically crystalline [3, 4]. These splats form the lamellar main structure of a coating while the coating exhibits also defects e.g. voids and often also some cracks [2, 3]. During the cooling at least some vertical cracks are rather easily formed in the thermally sprayed ceramic coating, which is especially problematic in electrical insulation materials. The length and the amount of cracks play an important role in the dielectric properties of the ceramic coatings. Especially, the DC breakdown strength has been found to decrease when long vertical cracks exhibit in a ceramic coating [5].

In this paper, the studied coatings are deposited either by high-velocity oxygen fuel (HVOF) process, which is a flame spray method in which a fuel gas (e.g. ethylene) and oxygen are used to create a high temperature combustion jet, or by plasma arc process. The main difference between the above processes is that the temperature of the flame in HVOF spraying is much lower (~3100 °C) than that of the plasma arc (~5500 °C) in plasma spraying [2, 3]. On the other hand, the particle velocity is much higher in the HVOF process (610–1060 m/s) than in the plasma process (240 m/s) [2], [6]. Accordingly, HVOF process typically results in a very dense and well-bonded coating suitable for many applications [2, 3].

Manuscript received on 13 July 2016, in final form 19 October 2016, accepted 3 November 2016. Corresponding author: M. Niittymäki.

Previous studies on the dielectric properties of HVOF and plasma sprayed Al_2O_3 and $MgAl_2O_4$ coatings have been focused on the short-term progressive breakdown strength, DC resistivity at low electric fields, and relative permittivity and dielectric losses [7–14]. Our previous studies have shown that thermally sprayed ceramic coatings exhibit strong non-ohmic conductivity starting from very low electric field strengths (~1 V/µm) originating from the special microstructure of the ceramic coatings [10, 11, 13]. However, our previous measurements on the conductivity were limited to low electric fields of ~5 V/µm or less due to the limitations of the measurement setup [10, 11, 13]. In order to study the DC conductivity of the ceramic coatings up to breakdown fields, a new measurement system has recently been developed and applied in the DC conductivity analysis of a HVOF sprayed alumina coating [15].

Typically, the DC conduction behavior of solid insulation materials can be explained by theoretical conduction mechanisms such as Schottky injection, Poole-Frenkel or space charge limited current (SCLC) mechanisms [16, 17]. Neusel et al. [18] and Talbi et al. [19] have observed that the DC conductivity of bulk alumina follows the SCLC mechanism. However, similar conductivity studies have not been conducted for thermally sprayed ceramic coatings. Typically, bulk alumina ceramic exhibits fully crystalline microstructure while ceramic coatings have amorphous and crystalline regions as well as voids and numerous interfaces. Due these differences, the DC conductivity of the coatings differs significantly from the bulk ceramic at low [10, 11, 13] and high [15, 18, 19] electric fields.

The aim of this paper is to study the DC conductivity over the full range from low electric fields up to breakdown fields for several different thermally sprayed ceramic coatings. In addition, the DC conduction mechanism is analyzed in detail. Moreover, the breakdown behavior of the coatings is studied utilizing linearly increased (short-term) test voltage and step-wisely increased voltage in order to get an indication of the possible short-term degradation of the coatings.

2 EXPERIMENTAL

2.1 MATERIAL CHARACTERZATION

Six different (Al_2O_3 or Al_2O_3/MgO) powders were thermally sprayed by the HVOF technique at VTT. In addition, one Al_2O_3 powder was deposited using atmospheric plasma spraying technique. Detailed information of all the studied coatings is listed in Table 1. The commercial alumina powders utilized in the coatings HVOF5, HVOF6 and Plasma differed slightly from each other. However, the same experimental alumina powder was used in coatings HVOF7–11 while the amount of MgO was varied from 0 to 50%. All the coatings were sprayed on 2.5 mm thick stainless steel substrates which were grit-blasted before coating deposition.

Figure 1 presents the cross-section images of the studied coatings taken by scanning electron microscope (SEM) with backscattered electron detector. The porous nature of the coatings as well as the lamellar structure can be seen from the images. The porosities of the coatings were defined by image analysis using the cross-sectional micrographic images of either optical microscope (OM) or SEM with two detectors: secondary electron detector (SE) or backscattered electron detector (BSE). In image analysis, the image magnification was 320 in OM images and 1000 in SEM images. The defined porosity values are listed in Table 1**.** In addition, the gas (nitrogen) permeability (GP) was measured for the coatings in accordance with ISO 4022 standard. Typically, high gas permeability indicates high porosity. Especially, this relationship can be noticed when comparing the OM and SEM/BSE porosities to the gas permeabilities. The porosities of plasma alumina defined from SEM images are at a higher level than the values of HVOF aluminas which is understandable due to the higher particle velocity in the HVOF process [2, 3].

Sample thicknesses were measured with Elcometer 456B device from the electrode areas (Ø=11 mm or Ø=50 mm depending on the test). The average thicknesses and standard deviations of the coatings are listed in Table 1 (10 parallel measurements from the 50 mm electrode area). In addition, the coating thicknesses were also determined from the cross-section images taken by optical micrographs and the obtained values are given in Table 1. The standard deviations of the thicknesses are quite large which may partly be due to the grit blasting of the coating substrate and consequently uneven lower surfaces of the coatings [11]. In addition, the spraying process itself does not produce fully smooth coating surface which also partly explains the thickness deviation. Anyhow, the thicknesses obtained by the two methods were at similar level although separate samples were utilized for the measurements.

2.2 DIELECTRIC CHARACTERIZATION

2.2.1 SAMPLE PREPARATION

For DC conductivity measurements below 1 kV voltages, a round electrode (Ø=50 mm) was painted on the sample surface using a special silver paint (SPI High Purity Silver Paint). In addition, a shield electrode was painted around the measuring electrode to prevent possible surface

Table 1. Studied materials and their properties.

Sample	Powder composition	Porosity				Thickness (µm)		
		OM (%)	SEM/SE (%)	SEM/BSE (%)	GP (nm^2)	From cross-section image	From magnetic measurement	SD
HVOF5	commercial Al_2O_3 (agglomerated & sintered)	6.0	1.7	3.7	11.1	215	228	6.2
HVOF6	commercial Al_2O_3 (fused)	1.4	1.4	1.4	3.2	333	307	6.1
HVOF7	experimental Al_2O_3 (agglomerated & sintered)	2.9	1.0	2.6	7.7	255	237	10.2
Plasma	commercial Al_2O_3 (fused)	2.3	2.4	3.6	–	245	271	11.4
HVOF8	90 % Al_2O_3 – 10 % MgO (agglomerated & sintered)	3.0	1.2	3.1	4.8	195	193	8.0
HVOF9	75 % Al_2O_3 – 25 % MgO (agglomerated & sintered)	2.5	1.2	3.1	3.9	190	184	7.9
HVOF11	50 % Al_2O_3 – 50 % MgO (agglomerated & sintered)	2.4	1.1	3.8	6.3	257	215	2.4

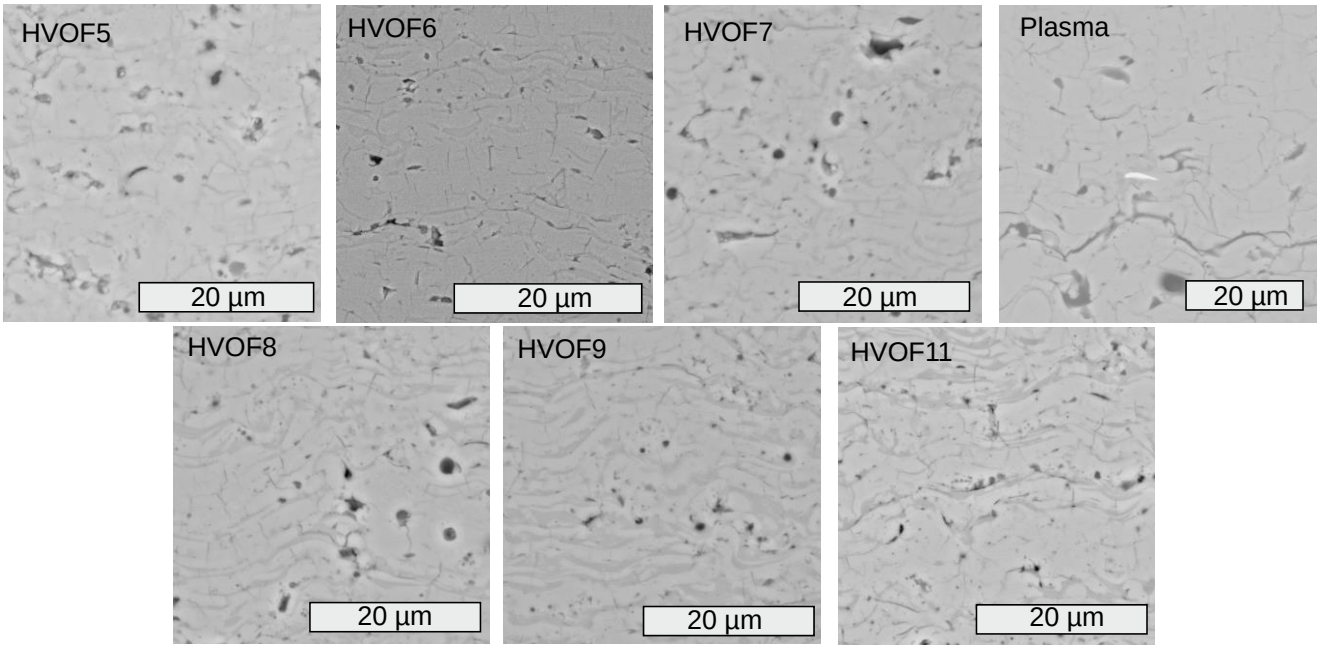

Figure 1. SEM/BSE cross-sectional images of the studied coatings at 1000× magnification. The ligth gray image areas correspond to the crystalline regions while the dark gray areas correspond to the amorphous regions. The black image areas are voids indicating the porosity of a coating.

currents, see Figure 3. For the DC conductivity and breakdown measurements above 1 kV, smaller silver painted electrodes (Ø=11 mm) were prepared, see Figure 3. In this setup, no guard ring was used. According to preliminary experiments, the surface currents were evaluated to be rather small compared to the current through the sample and the variation between the parallel samples. Our previous study indicated that the silver paint does not penetrate into the coating [12]. After painting the electrodes, the samples were at first dried at 120 °C for two hours followed by conditioning in a climate room at 20 °C, RH 20% for at least 12 h before the measurements. All the measurements were also performed at these controlled conditions in the climate room.

2.2.2 DC CONDUCTION MEASUREMENTS

DC conductivity was measured using two different measurement setups due to the wide measurement range and sensitivity required for the leakage current measurements. Below 1 kV voltages, the DC conduction current measurements were performed using Keithley 6517B electrometer. The measuring electric field was varied from 0.1 V/µm to ~4 V/µm and the measurement period for each voltage level was 1000 s. During each measurement period, the pure constant DC conduction current was normally reached. During the measurements, a stainless steel electrode (Ø=50 mm) was placed on the top of the silver painted area on the coating sample while the stainless steel substrate of the sample acted as the other electrode. The current density was determined from the average of the stabilized DC current measured over 990–1000 s after the voltage application. All the measuring arrangements were in accordance with the standard IEC 60093 [20].

Above 1 kV voltages, the DC conductivity was studied by increasing the voltage step-wisely in 250 V/10 min steps starting from 250 V until breakdown occurred. During the measurements, a stainless steel rod electrode (Ø=11 mm, edge rounding 1 mm) was placed on the top of the silver painted area on the coating sample while the stainless steel substrate of the sample acted as the other electrode. In order to avoid surface flashovers at the highest test voltages (in practice for all HVOF coatings), a plastic cylinder with an O-ring sealing towards the coating surface was clamped around the measuring electrode (Ø=11 mm) to extend the surface distance over the solid insulation. The typical oil immersion –method cannot be used due to the porous nature of the coatings [12]. The schematic figure of the measurement circuit as well as the test bench is presented in Figure 2. The sample current was measured throughout the tests by a shunt resistor (1 MΩ or 10 kΩ depending on the signal level) and a Keithley 2001 digital multimeter. The voltage source control and data recording was performed using LabVIEW-based software. The voltage source was Keithley 2290-10 power supply (U_{max}=10 kV).

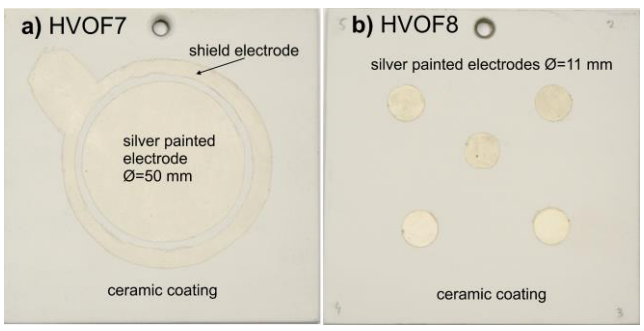

Figure 3. Photographs of the electrode arrangements utilized in the conductivity measurements below 1 kV (**a**) and above 1 kV (**b**) voltage levels. The photographs were taken after the measurements.

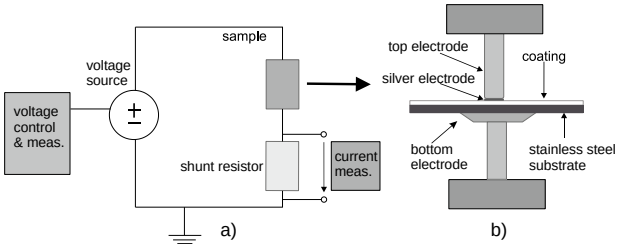

Figure 2. Schematic figure of the measurement circuit and test bench used in DC conductivity measurements above 1 kV.

2.2.3 BREAKDOWN VOLTAGE MEASUREMENTS

Breakdown strengths of the materials were measured by using the above described step-wise tests as well as by utilizing linear ramp tests (ramp rate of 100 V/s throughout the test). The measurement arrangements were otherwise similar to the step-tests but the voltage source was Spellman SL1200 (U_{max}=20 kV) and the voltage was measured using a resistive voltage divider (Spellman HVD-100-1, division ratio 10000:1) [12]. Dielectric breakdown strength (DBS) of a coating was calculated by dividing the breakdown voltage by the corresponding coating thickness at the painted electrode (∅=11 mm) location. Despite obvious edge field enhancement at the edges of the painted electrodes, the breakdown locations were noticed to be distributed reasonably well along the electrode area. This is supposed to be caused by the rather high deviations in the breakdown strength.

2.2.4 STATISTICAL ANALYSIS OF THE BREAKDOWN DATA

Typically, the dielectric breakdown strength of solid materials is Weibull distributed and due to this the results were fitted to this distribution. The cumulative density function of a two-parameter Weibull distribution is given as

$$F(x) = 1 - \exp\left\{-\left(\frac{x}{\alpha}\right)^{\beta}\right\}, x \geq 0, \quad (1)$$

where $F(x)$ is the breakdown probability, x is the measured breakdown strength (V/µm), α is the scale parameter (V/µm) and β is the shape parameter. The scale parameter represents the breakdown strength at the 63.2% failure probability and the shape parameter indicates the slope of the theoretical distribution. The statistical analysis was performed using Weibull++® software and the Maximum Likelihood method was used in the parameter estimation.

3 RESULTS AND DISCUSSION

3.1 GENERAL BEHAVIOR OF DC CONDUCTION CURRENTS

Figure 4a-4g presents the measured currents for each studied coating sample as a function of time when the voltage was increased step-wisely until breakdown. The breakdown strengths defined from these measurements are presented in Figure 4h. It can be noticed that the coatings exhibit strong non-linear voltage-current relationship and quite large deviation in breakdown results as well as in the conduction currents between the parallel samples. It can be observed from Figure 4 that the coatings exhibit a 'transition-field' region where highly non-ohmic conductivity is increasing to a new current level until breakdown occurs.

The focus of this study is to compare the DC conductivities of the different coating materials in a more general sense rather than to determine the DC conductivity of only one type of coating material in detail using very large number of parallel samples. The conduction current behavior of the HVOF coatings sprayed using commercial alumina powders (HVOF5 and HVOF6) is quite similar although the absolute current values differed. In addition, it can be noted that one of the samples of HVOF5 coating differs significantly from the other four samples. The conductivity of plasma sprayed alumina generally is at a similar level with HVOF6 coating. However, the current of plasma coating changes more rapidly in the 'transition-field' region with non-ohmic conduction than in the HVOF coatings. The conduction current behavior of HVOF7 and HVOF8 is very similar which is understandable due to the similar amounts of MgO (HVOF7 0%, HVOF8 10%) added in the same Al_2O_3 powder. The conductivity of HVOF9 (25% MgO) is very similar with alumina HVOF5 although the actual current level of HVOF9 is lower than the current of HVOF5. Three of five parallel samples of HVOF11 (50% MgO) did not break down until the maximum voltage of the power supply was reached. In addition, the current levels of those three samples were clearly lower than the currents of the samples which broke down. Although there are clear general differences between the materials, the typical current levels just prior the breakdown events were roughly at a level of ~10^{-6} A for all the coatings.

3.2 ANALYSIS OF THE CONDUCTION CURRENTS VERSUS ELECTRIC FIELD

In order to evaluate the conduction processes of the coatings in more detail, current densities of the studied coatings were determined as a function of applied electric field. Although the steady-state current level was not reached at each applied voltage level (this can be especially seen in the 'transition field' region, see Figure 4), the current densities of the materials were defined from the mean values of the current at the end of each voltage step (550–580 s). It should be underlined that in 'the transition fields' the defined current densities do not thus represent DC conductivity implicitly. Figure 5 presents the defined current densities of five parallel samples of each coating as a function of applied electric field. In addition, the average current densities of the five parallel samples are presented. Anyhow, for HVOF5 the average current density was defined only from four samples because one of the five samples exhibited totally different conduction behavior.

As it can be noticed from Figure 5, the current densities measured using the low (L1) and high (H1–H5) field measurement setups differed to some extent. This is most probably because the sensitivity of the high field measurement setup was insufficient at the lowest test fields (see the high noise in the lowest test voltages in Figure 4). Separate samples were utilized at low and high field measurements. Quite large deviation between the parallel samples (H1–H5) can be seen and it can further explain the difference. As it was mentioned previously, the materials are also in a 'transition-field' region with non-ohmic conduction when the high and low field setups are comparable. In this region, the currents did not fully reach the steady-state level during the test period of 10 min and thus the defined values did not represent the true DC conductivity.

In order to further study, the differences between the materials, the experimental data were plotted as log *(J)* versus log (*E*) where approximately straight lines with different slopes at different regions of field strengths may be obtained. Least-square technique was utilized to define the best fits for the conduction currents, and thus to define the slopes for each region. Table 2 presents the defined slopes

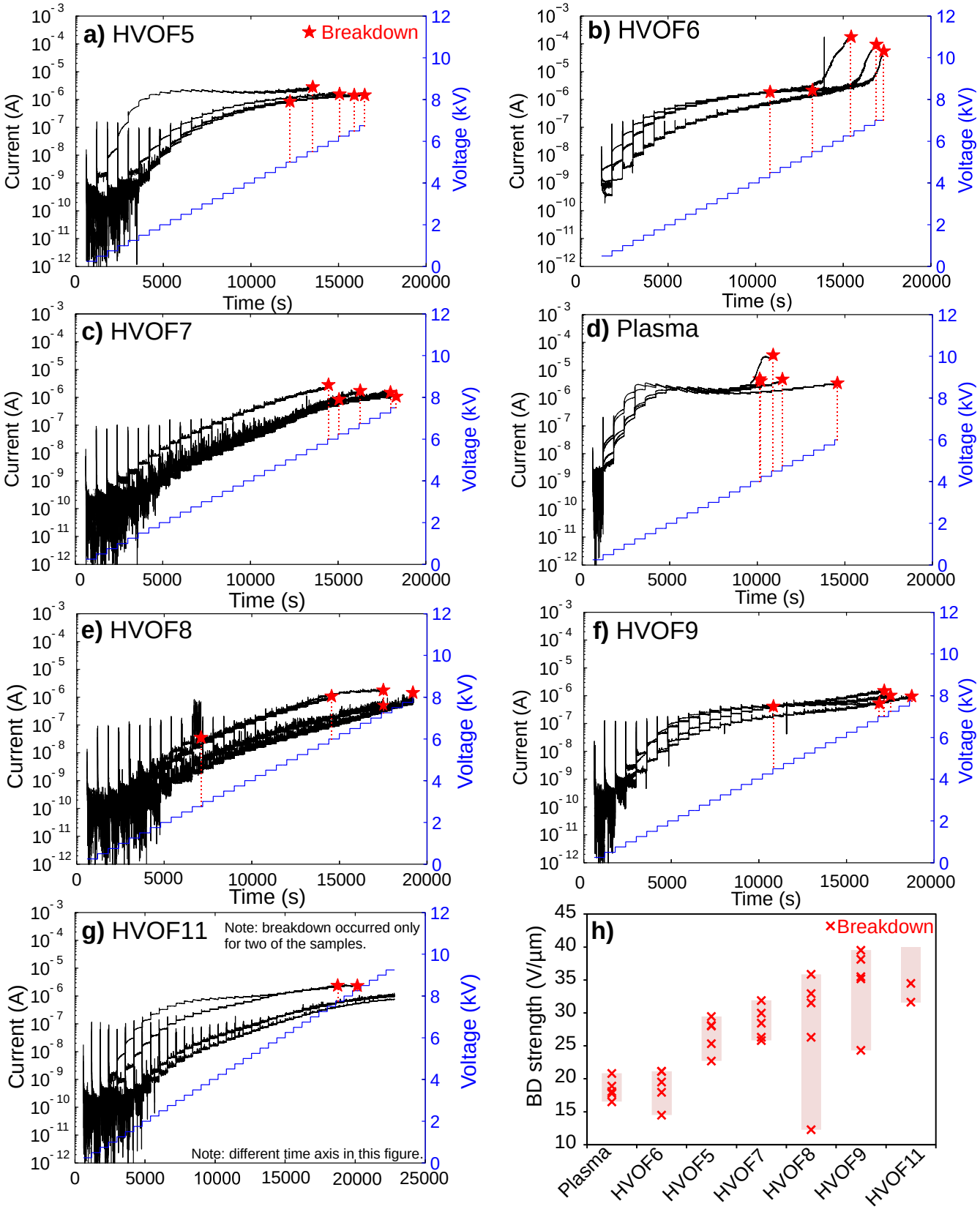

Figure 4. a–g Measured DC currents of the studied materials as a function of time. The start voltage was 250 V which corresponds the electric field of ~1 V/µm. The red stars and the dashed lines indicate the occurrence of breakdown (current and voltage, respectively). It should be underlined that breakdown occurred only for two out of five samples for HVOF11 since the maximum voltage level of the power supply was reached. **h)** The breakdown strengths of the studied coatings in which the cross presents individual breakdown measurement and the bar indicates the deviation between the minimum and maximum strengths. For HVOF11 the upper limit of the bar presents the maximum electric field reached for the samples which did not break down during the tests.

of the mean current densities in different areas as well as the estimated transition electric fields between the different regions.

At low field levels (Area 1), all the studied coatings are obviously ohmic because the defined slopes are close to unity indicating that electric field/voltage is directly proportional to the current. The estimated transition field to non-ohmic region varies between the materials. The lowest field (~0.5 V/µm) is noticed for alumina coatings HVOF6 and Plasma. Slightly higher transition field (~1 V/µm) can be observed for the other commercial HVOF sprayed alumina (HVOF5) but the highest transition field (~2 V/µm) of the alumina coatings is obtained for experimental alumina HVOF7. The transition field of HVOF8 is the same as it is

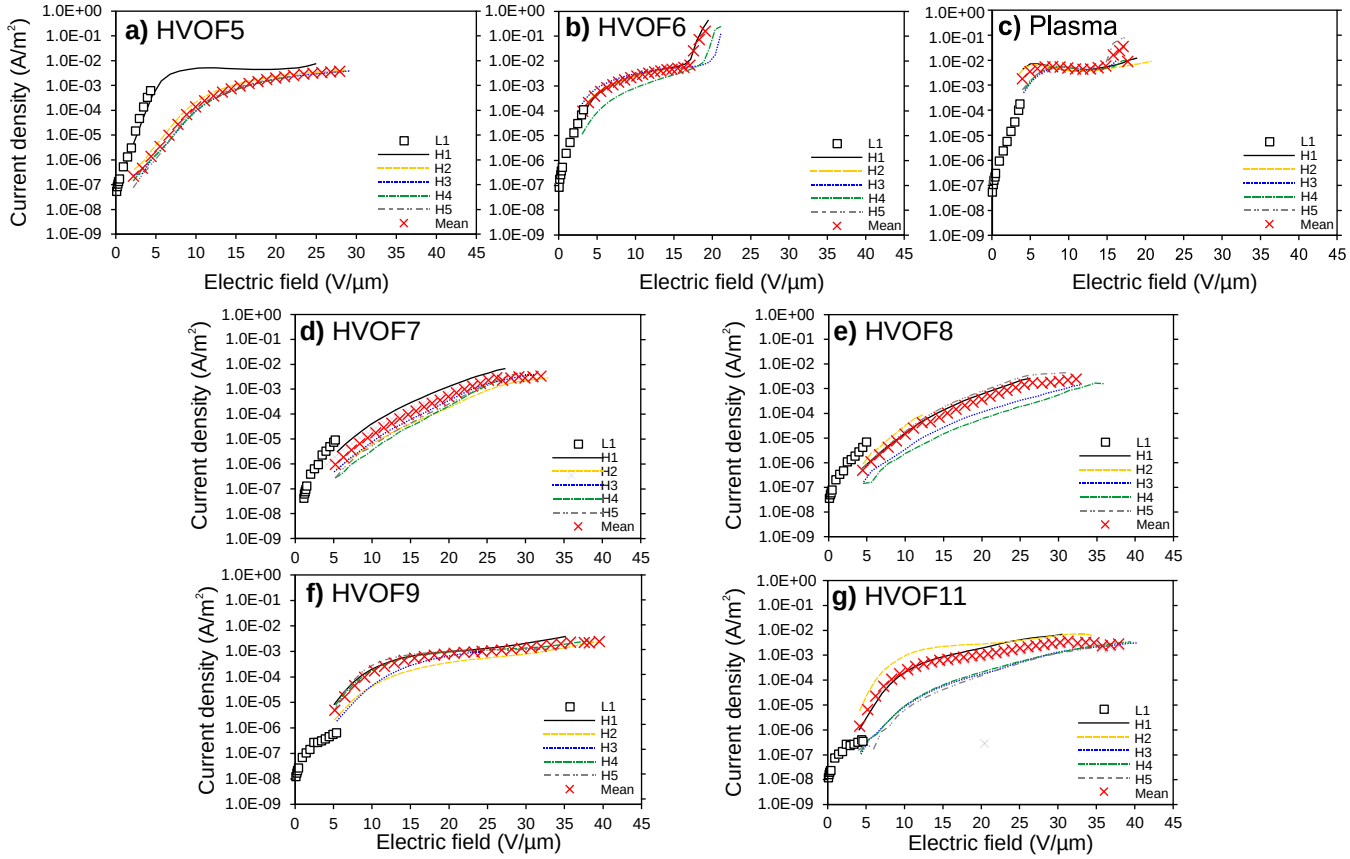

Figure 5. DC conduction currents as a function of applied electric field for the studied coatings. The squares (L1) represents the currents measured using Keithley electrometer and the lines (H1–H5) presents the conduction currents recorded using the above 1 kV measurement setup. The crosses represent the average current densities defined from the five parallel conductivity measurements performed until breakdown, except for HVOF5 the average current density is defined from four parallel measurements.

for HVOF7 probably due to the almost similar powder composition (10% MgO versus 0% MgO). The highest transition field (~4 V/µm) is noted for the coatings with higher amount of MgO: HVOF9 (25% MgO) and HVOF11 (50 % MgO).

In the next region (Area 2), the conductivities of the coatings are highly non-ohmic since the defined slopes vary from 2.8 to 6.2. As it was already mentioned earlier in this 'transition field' region the currents did not fully stabilize during the DC step-stress periods (10 min), instead they were still increasing at the end of the periods. Thus, the real levels of stabilized DC current would have been slightly higher than the reported values, and the above mentioned slopes would have been correspondingly higher as well. All in all, it can be concluded that a considerable transition from ohmic conduction state to another state occurs in this region. Typically, the transition field of HVOF coatings from Area 2 to Area 3 is ~10 V/µm. However, the transition field of HVOF5 is higher (17 V/µm) but in [15] the transition field of HVOF5 has been reported to be 10.5 V/µm although the DC stress period was only 6 min. This indicates that the conductivities of the parallel samples of a coating material deviate notably. The lowest transition field is noted for plasma sprayed alumina coating (5.9 V/µm). The differences in conductivities and breakdown strength between HVOF and plasma coatings may be linked to their different microstructure (Figure 1) caused by the different spraying temperatures and powder particle velocities in the spraying processes.

In Area 3, the defined slopes are roughly two indicating that the current density is proportional to the square of the electric field. However, HVOF7 and HVOF8 exhibit similar but clearly higher slopes (~5) than the other HVOF coatings, and thus these two coatings exhibit similar behavior as the other coatings in the previous area. In addition, the conductivity of plasma alumina differs from the HVOF

Table 2. Estimated transition electric fields and corresponding slopes of the mean current densities (log–log scale) for the studied materials as well as the relative permittivity measured at the voltage of 200 V_{peak}. The detailed measurement procedure of the permittivity measurements is presented in [11–13], [15].

	Area 1		Area 2		Area 3		Area 4		Permittivity
Sample	*E* (V/µm)	Slope	*E* (V/µm)	Slope	*E* (V/µm)	Slope	*E* (V/µm)	Slope	ε_r (at 1 kHz)
HVOF5	0 – 1.0	1.1	1 –16.6	5.7	16.6 – 28	2.2	–	–	9.1
HVOF6	0 – 0.5	1.1	0.5 – 8.6	3.4	8.6 – 17.1	1.8	17.1–	21.7	8.5
HVOF7	0 – 2.0	1.2	2 – 10.5	2.8	10.5 – 24.1	5.3	24.1–	1.3	8.3
Plasma	0 – 0.5	1.0	0.5 – 5.9	4.3	5.9 – 13.9	−0.3	13.9–	12.2	9.8
HVOF8	0 – 2.0	1.1	2 – 7.8	2.8	7.8 – 26.6	4.9	26.6–	2.6	8.5
HVOF9	0 – 3.9	1.2	3.9 – 10.3	4.5	10.3 – 37.6	1.6	–	–	8.5
HVOF11	0 – 4.1	1.1	4.1 – 9.4	6.2	9.4 – 26.1	2.1	26.1–	1.1	8.4

coatings because the plasma reached ohmic level in this area but this may be noticed only by visual evaluation because the obtained slope has negative value due to differences between the parallel samples current density values.

Breakdowns occurred for the alumina coating HVOF5 and spinel HVOF9 in Area 3 but for the rest of the materials the breakdowns occur in Area 4. Although a rapid current increase before breakdown has previously been observed for alumina HVOF5 in [15], no such increase in conduction current is observed for HVOF5 in this study. However, similar rapid current increase is seen for some of the samples of alumina (HVOF6 and Plasma) because the obtained slopes in Area 4 are very high (see Figure 4 and Figure 5).

Throughout the tests, the conduction behavior of the coating HVOF8 (10% MgO) is very similar to the alumina HVOF7 (0% MgO) but in Area 4 the conductivity of HVOF7 is ohmic (slope ~1) while the conductivity of HVOF8 is equal to the square of electric field (slope ~2). Thus, it may be concluded that adding 10% MgO to the Al_2O_3 has only effect when the applied electric field is above 25 V/µm. The conduction behavior of the other two spinel coatings (HVOF9, 25% MgO and HVOF11, 50% MgO) is very similar throughout Areas 1–3. However, the breakdown occurred for HVOF9 in Area 3 while the breakdowns of HVOF11 occurred in Area 4 in which HVOF11 exhibits ohmic conduction behavior (slope ~1). Thus, it seems that the amount of MgO (25 or 50%) has influence on the conduction behavior only when the field is above ~26 V/µm.

3.3 MATERIAL DEGRADATION

Our previous studies [10] have shown that the DC resistivity of a HVOF sprayed experimental spinel coating decreased remarkably when the resistivity as a function of electric field (~0.1–3 V/µm) was repeated. Due to these permanent changes, the conductivity measurements below 1 kV were repeated for some of the samples in this study (two aluminas: HVOF5 and HVOF7, and one spinel: HVOF11) in order to identify possible permanent changes at low electric fields. The selected coatings represent the conduction behavior of the coatings in general manner.

Figure 6 presents the original DC conduction currents of the above coatings as a function of electric field together with the results of repeated measurements made later on.

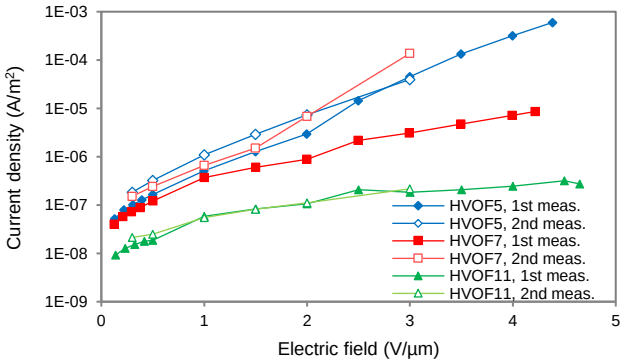

Figure 6. DC conduction currents as a function of electric field for two alumina coatings (HVOF5 and HVOF7) as well as one spinel coating (HVOF11). The data of 1st measurement is same as it has been shown in Figure 4.

The time between the measurements was several months and during that time the samples were kept in a desiccator at room temperature/low relative humidity to avoid ageing. It can be noticed that some permanent changes occurred for the experimental alumina coating (HVOF7) at already low electric fields since the conductivity increases remarkably during the second measurement period. The conductivity of the commercial alumina (HVOF5) also increased slightly during the second measurement time but the difference is not so significant. No permanent changes occurred for the spinel coating (HVOF11).

Because these permanent changes occur already at very low electric fields, it is evident that it is not meaningful to perform conduction mechanism analysis for all the studied materials. In order to carry out the conduction mechanism study for HVOF5 and HVOF11, the conductivity measurements were also repeated at high fields to ensure that no permanent changes/degradation occur in the materials. Three more samples of alumina HVOF5 were prepared and conductivity measurements were made for these samples with steps of 500 V/10 min until the voltage level of 3500 V was reached. The voltage corresponds to the electric field of ~15 V/µm which is approximately half of the breakdown strength of the HVOF5. The measurements showed that no permanent changes occur for the samples of HVOF5 when the measurements were repeated on the next day.

The procedure of conductivity measurements for HVOF11 was similar but the measurements were performed until the voltage level of 5500 V was reached. This level corresponds to the field of ~22 V/µm which is roughly half of the breakdown strength of HVOF11. The measurements were performed for the samples that did not break down in the step tests with 250 V/10 min steps. These measurements indicate that the current densities are at similar levels when the measurements were repeated two or three times (500 V/10 min).

During the first applications of higher electric fields, permanent changes in the conductivity may occur for some of the coatings. The permanent changes might be due to the changes occurred in the interfaces of amorphous-crystalline regions of the coatings.

3.4 CONDUCTION MECHANISMS ANALYSIS

In order to evaluate the dominant conduction mechanism of thermally sprayed ceramic coatings, the measured conductivity data are analyzed in accordance with several theoretical conduction mechanisms despite the fact that the steady-state current level was not reached at each voltage level, especially in the ‘transition-field’ region. Because the possible dominating conduction mechanism of thermally sprayed ceramics is not so evident, all theoretical conduction mechanisms are discussed even though some of the mechanisms occur only at very high electric fields for other materials such as polymers [16], and are thus not relevant for thermally sprayed ceramic coatings. The conduction mechanism study is only carried out for alumina HVOF5 and spinel HVOF11 for which no material degradation was noticed and the measured conduction behavior can thus be considered to be stable.

Charge injection from electrodes can be described either by Schottky or Fowler-Nordheim injection mechanisms which both occur at very high fields for polymers, e.g. the latter takes places ~10^9 V/m and the former one occurs slightly lower fields [16, 17]. Although thermally sprayed ceramic coatings exhibit significantly lower breakdown strengths than polymers, the Fowler-Nordheim plots (log (J/E^2) versus $1/E$) were made for HVOF5 and HVOF11 [21, 22]. The obtained plots indicate that Fowler-Nordheim tunneling can be excluded as the dominating conduction mechanism for the studied thermally sprayed ceramic coatings because the slopes differed clearly from those reported in [21, 22] where the Fowler-Nordheim tunneling occurred for the studied materials.

In the Schottky analysis, the measured data is plotted as ln (J) versus $E^{1/2}$ (Schottky plot) which results a straight line where theoretical value of relative permittivity can be evaluated. Thus, the comparison between the theoretical and measured high frequency permittivities can be made. For both coatings (HVOF5, HVOF11) the relative permittivities defined from the Schottky plot are ~70% smaller than the measured ones (Table 2), and thus the pure Schottky injection can also be excluded as the dominating conduction mechanism of the thermally sprayed coatings.

At high electric fields, one of the bulk-limited conduction mechanisms is Poole-Frenkel where the theoretical relative permittivity can be defined from the slope of the Schottky plot (ln (J) versus $E^{1/2}$). The physical base of Poole-Frenkel model is very simplified and the analysis must be made as an-order-of-magnitude calculation [16]. Although this consideration is made, the defined theoretical values are ~95% smaller than the measured ones. Thus, it can be concluded that the Poole-Frenkel conduction mechanism is not the dominating one for the ceramic coatings.

Space charge limited current (SCLC) mechanism is one of the bulk limited conduction mechanisms and it describes how the conduction current behavior changes with increasing applied electric field [16, 17]. In order to validate this mechanism, experimental J–E data can be plotted in double logarithmic scale (see Figure 7) [16, 17]. According to this mechanism, at low field strengths (field below the transition field, E_{TR}) the voltage-current relation is ohmic due to the thermally generated carriers [16, 17]. The current density is thus directly proportional to the voltage. Correspondingly, the slope is unity in a plot of log J – log E [16, 17].

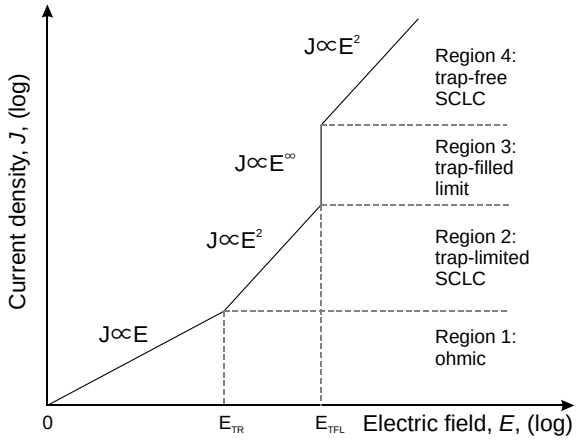

Figure 7. Relationship between electric field and current in accordance with the space charge limited current –theory. The figure is revised from [16].

At higher fields (Region 2), the conduction is no longer ohmic because charge can inject from electrode into the bulk and it has difficulties to move further through the material [16, 17]. Thus, a space charge is formed in vicinity of the electrodes and throughout the bulk and this charge will limit the further movement of charges which is known as SCLC [16, 17]. When the applied field has reached the level of E_{TR} (see Figure 7), the space charge limited current dominates over the ohmic component [16, 17]. The current is thus proportional to the square of electric field and the slope is two in a plot of log J – log E (Figure 7). When the applied field has reached the trap-filled limit field, E_{TFL}, all the traps in the dielectric are filled and the slope increases from two (see Region 3 in Figure 7) to infinity. At the fields above E_{TFL}, the trap-free space charge conduction might take place and the slope is two (Region 4 in Figure 7) if the breakdown did not occur before this region was reached [16].

It has been reported in [18, 19] that a bulk alumina ceramic follows the SCLC mechanism. However, the conductivities of alumina HVOF5 and spinel HVOF11 coatings do not fully follow the SCLC theory since after the initial ohmic region (Area 1 in Table 2) the conductivity is not proportional to the square of the electric field as indicated by the calculated slope of ~6 (Table 2). After this region, the slope should be higher than two in accordance with the SCLC theory (Region 3 in Figure 7) but the slopes of the coatings are ~2. According to the SCLC theory, the slope should be two again in the last area (Region 4 in Figure 7) but the slope of HVOF11 is ~1 in Area 4 indicating ohmic behavior. It can be concluded that the studied thermally sprayed ceramic coatings either do not follow or follow only partly the SCLC theory unlike the sintered alumina [17, 18]. The difference in the conduction behaviors of the bulk and the thermally sprayed alumina is most probably due to their different microstructures. Bulk alumina exhibits fully crystalline structure while the thermally sprayed coatings have lamellar structure consisting of both amorphous and crystalline areas as well as voids and defects (Figure 1). Due to above facts, the coatings most probably exhibit a variety of trap levels which partly explains the deviation of the performance from the ideal SCLC theory.

A thermally sprayed coating should be considered as an insulation system consisting of different regions which exhibit different dielectric properties. Thus, it can be speculated that the amorphous regions probably have higher conductivity than the crystalline regions. The differences in conductivity and the resulting uneven field distribution might be the reason why the coatings followed only partly the SCLC theory. Although there are many uncertainties, it can be speculated that thermally sprayed coatings could follow the SCLC theory as follows:

- At low electric fields (Area 1), the conductivity is clearly ohmic. Since the amorphous regions most probably exhibit higher conductivity than the crystalline regions, the electric field concentrates on the crystalline regions. Thus, the conduction behavior

of a coating is dominated by the conductivity of the crystalline regions.

- At higher electric fields, charges start to collect into the interfacial areas and traps forming space charge. When a certain transition electric field, E_{TR}, is reached, the space charge limited current dominates over the ohmic component in the crystalline-amorphous interfaces of a coating. Theoretically, the current density is proportional to the square of electric field when there is only one trap depth in the material. In the coatings, the microstructure varies along the material and due to this the E_{TR} and the current density changes are not as ideal, instead the changes take place 'smoothly'.
- When the conductivity increases in the crystalline regions, this also changes/equalizes the electric field distribution between the crystalline and amorphous regions at the same time. Due to this, at first the current is limited and is increasing with a slope lower than two but after a while the electric field is more concentrated on the amorphous regions, and thus the current is increasing strongly with a slope higher than two. This can occur since the transition field (E_{TR}) of amorphous regions is expected to be lower than the transition field of the crystalline regions due to their different conductivities.
- After this transition field range where a new electric field distribution is formed for a coating by the SCLC currents of amorphous and crystalline regions, the current of a coating system is increasing with a slope of ~2.

At higher test voltages prior to breakdowns, partial breakdowns of certain regions are suggested to occur. Just before breakdowns, rapid current increase was measured for certain coatings (HVOF6, Plasma). This is most probably caused by partial breakdowns e.g. in the amorphous regions and/or at the interfaces between the splats which may take place because the trap filled limit (E_{TFL}) of that region is reached. According to the SCLC theory, a sudden fast current increase occurs, when the E_{TFL} is reached. However, this current increase should lead to breakdown very rapidly [16]. As the current increase of the coatings did not occur as rapidly, it is suggested that the breakdown for some of the coatings proceeded partially, and this way the breakdown process was delayed.

3.5 DC BREAKDOWN STRENGTH

Figure 8 presents the DC breakdown strengths of the coatings when the voltage was increased with 100 V/s linear ramp rate. Two-parameter Weibull distributions were fitted to the breakdown data. The Weibull parameters α and β are listed in Table 3 along with the breakdown strengths at the breakdown probabilities of 10% and 90%.

The lowest breakdown strength (Weibull α) is obtained for the plasma sprayed alumina. In addition, the deviation between the parallel samples is large (the difference between the breakdown probability of 10% and 90%). The Weibull β of Plasma also is clearly lower than the Weibull β of HVOF coatings which show very similar values (see the inset in Figure 8b). The lowest breakdown strength (Weibull

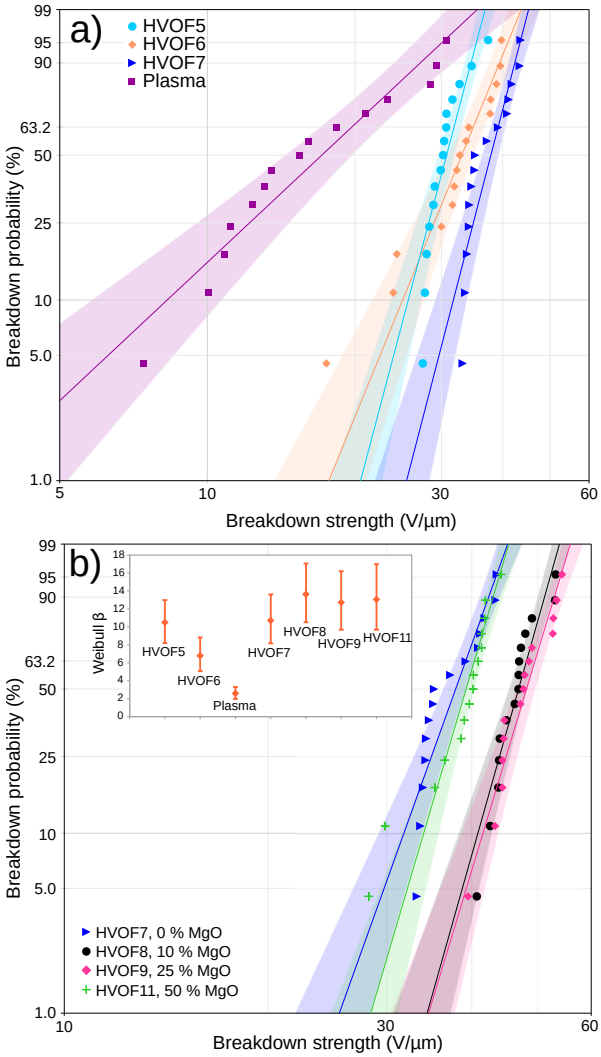

Figure 8. DC breakdown strength of the coatings when the voltage was increased linearly at the ramp rate of 100 V/s to breakdown. The shaded areas represent 90% confidence bounds. The inset shows the Weibull β and its 90% confidence limits.

Table 3. Weibull parameters α and β as well as the breakdown strenghts at the breakdown probabilities of 10% and 90%.

	Plasma	HVOF5	HVOF6	HVOF7	HVOF11	HVOF8	HVOF9
10%	8.3	25.7	25.0	31.7	33.9	40.8	41.5
α	19.7	31.8	34.8	39.2	40.3	48.1	49.6
90%	27.2	34.5	39.4	42.3	43.0	51.2	52.9
β	2.6	10.5	6.8	10.7	13.1	13.6	12.7

α) for the HVOF coatings is obtained for HVOF5 and only slightly higher value for HVOF6 which both were manufactured from different commercial alumina powders. The experimental alumina coating (HVOF7) exhibits the highest breakdown strength of the alumina coatings and the breakdown strength is at a similar level with HVOF11 (50% MgO). Typically, the breakdown strength of HVOF alumina coatings are significantly lower than the breakdown strength of HVOF spinels [8, 13]. The highest breakdown strengths are obtained for HVOF8 (10% MgO) and HVOF9 (25% MgO) which practically exhibit equal breakdown strengths (Weibull α).

Due to the rather high deviation of parallel breakdown results, it is difficult to distinguish the exact effect of MgO content on the breakdown strengths. However, it seems that adding MgO in Al_2O_3 improves the breakdown strength, and

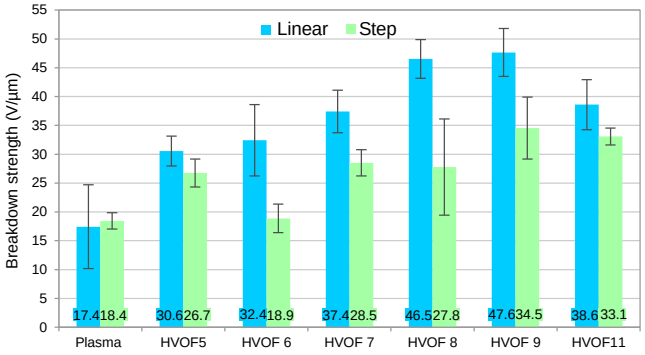

Figure 9. DC breakdown strength of the coatings from linear ramp rate and from step measurements. The results from step tests are the same as what has been presented in Figure 4h). The error bar represents the experimental standard deviations of parallel measurements (15 test in linear ramp tests and two or five tests in step tests).

the amount of 25% gives the highest breakdown strength in step and linear tests (see Table 3, Figure 8 and Figure 9).

Other microstructural features, e.g. gas permeability which is related to the volumetric porosity of a coating, seem to affect the breakdown strength of the HVOF coatings deposited from experimental powders (HVOF7–HVOF11) more obviously than the amount of MgO [5]. The higher gas permeability results in lower breakdown strength since the highest breakdown strength was obtained for HVOF9 (GP 3.9 nm^2) and the lowest for HVOF7 (GP 7.7 nm^2) [5]. Because HVOF11 (50% MgO) has quite similar breakdown strength and gas permeability with HVOF7 (0% MgO), it can be speculated that the gas permeability has a more profound effect on the breakdown strength than the MgO content [5]. However, the effect of gas permeability on the breakdown strength is not as evident when the comparison is made for all studied HVOF coatings since the gas permeability of the alumina coating HVOF6 (3.2 nm^2) is the lowest one of the HVOF coatings but the breakdown strength is not the highest one even though the comparison is only made between the alumina coatings. Anyhow, the HVOF5 coating (the other commercial alumina powder) exhibits higher gas permeability (11.1 nm^2) and slightly lower breakdown strength than the other commercial HVOF alumina coating (HVOF6). Although the difference between the breakdown strengths is not significant, it might be speculated that the difference is partly due to their different volumetric porosities.

Figure 9 presents the average breakdown strengths of the coatings when the voltage was increased either linearly or step-wisely. For plasma sprayed alumina the breakdown strength in step-test is practically same as the breakdown strength in ramp-test because the deviation between the parallel samples in linear tests is significant (see Figure 8a). For HVOF coatings, the step-test breakdown strengths are lower than the ramp-test breakdown strengths. The difference is from 3.9 V/µm (HVOF5) to 18.7 V/µm (HVOF8). It is understandable that the step-test breakdown strength is lower than the ramped one due to the clearly longer stress durations. The differences thus give an indication of the effects of electric stress duration and possible time dependent degradation of the coatings. An interesting continuation of this work would be long-term ageing testing for evaluating suitable service field strengths of the coatings.

4 CONCLUSIONS

In this study, the DC conductivities of several different thermally sprayed ceramic coatings were studied in order to determine the conduction behavior of the coatings in general manner. Although great differences in the conductivities of the different coatings were observed, it was seen that in all coating types the conduction currents reached similar level prior to the breakdown.

Thermally sprayed ceramic coatings exhibit a special lamellar microstructure consisting of crystalline and amorphous regions as well as voids and defects, while bulk ceramics exhibit fully crystalline structure. Due to this difference, their DC conductivities differ; thermally sprayed ceramic coatings exhibit strong non-linear conduction behavior already at low field strengths unlike bulk ceramics. In addition, as opposed to bulk alumina, the ceramic coatings do not follow or follow only partly the space charge limited current conduction mechanism while the bulk alumina has been reported to follow this mechanism. A possible conduction mechanism for the ceramic coatings was proposed based on the differences in the conductivities of the amorphous and crystalline regions of the coating which further causes an uneven electric field distribution in a coating.

Due to the large variations in the DC breakdown strength, it was difficult distinguish the exact effects of MgO content or porosity. However, it seems that the volumetric porosity has a more profound effect on the breakdown strength for the experimental coatings, higher porosity indicating lower breakdown strength. The step-test breakdown strengths of the coatings were lower than the ramp-test ones due to the clearly longer stress durations in step-tests which gives an indication of the effects of electric stress durations and possible short-term degradation of the coatings. An interesting continuation of this work would be long-term ageing testing for evaluating of suitable service field strengths of the coatings.

ACKNOWLEDGMENT

Nida Riaz and Juuso Kukkaro are greatly acknowledged for performing most of the DC conductivity measurements.

REFERENCES

[1] N. H. Menzler, F. Tietz, S. Uhlenbruck, H. P. Buchkremer, and D. Stöver, “Materials and manufacturing technologies for solid oxide fuel cells,” J. Mater. Sci., Vol. 45, No. 12, pp. 3109–3135, Feb. 2010.

[2] J. R. Davis, *Handbook of Thermal Spray Technology*, Vol. 3, USA, ASM International, 2004.

[3] L. Pawlowski, *The Science and Engineering of Thermal Spray Coatings*. Chichester, West Sussex, England: John Wiley & Sons Ltd, 2008.

[4] E. E. J. Young, E. Mateeva, J. J. Moore, B. Mishra, and M. Loch, “Low pressure plasma spray coatings,” Int. Conf. Metall. Coatings Thin Film., Vol. 377–378, pp. 788–792, 2000.

[5] M. Niittymäki, I. Rytöluoto, J. Metsäjoki, T. Suhonen, and K. Lahti, “Role of Microstructure in Dielectric Properties of Thermally Sprayed Ceramic Coatings,” IEEE 1st Int’l. Conf. Dielectr., 2016.

[6] V. V. Sobolec, J. M. Guilemany, and J. Nutting, *High Velocity Oxy-fuel Spraying Theory, Structure-Property Relationships and Applications*. The Institute of Materials, Minerals and Mining, Maney Publishing House, 2004.

[7] L. Pawłowski, “The relationship between structure and dielectric properties in plasma-sprayed alumina coatings,” Surf. Coatings

Technol., Vol. 35, No. 3–4, pp. 285–298, 1988.
[8] F. L. Toma, S. Scheitz, L. M. Berger, V. Sauchuk, M. Kusnezoff, and S. Thiele, "Comparative study of the electrical properties and characteristics of thermally sprayed alumina and spinel coatings," J. Therm. Spray Technol., Vol. 20, No. 1–2, pp. 195–204, 2011.
[9] F. L. Toma, L. M. Berger, S. Scheitz, S. Langner, C. Rödel, A. Potthoff, V. Sauchuk, and M. Kusnezoff, "Comparison of the Microstructural Characteristics and Electrical Properties of Thermally Sprayed Al_2O_3 Coatings from Aqueous Suspensions and Feedstock Powders," J. Therm. Spray Technol., Vol. 21, No. 3–4, pp. 480–488, 2012.
[10] M. Niittymäki, K. Lahti, T. Suhonen, U. Kanerva, and J. Metsäjoki, "Dielectric properties of HVOF sprayed ceramic coatings," IEEE Int'l. Conf. Solid Dielectr., pp. 389–392, 2013.
[11] M. Niittymäki, T. Suhonen, J. Metsäjoki, and K. Lahti, "Influence of Humidity and Temperature on the Dielectric Properties of Thermally Sprayed Ceramic $MgAl_2O_4$ Coatings," IEEE Conf. Electr. Insul. Dielectr. Phenomena, pp. 94–97, 2014.
[12] M. Niittymäki, K. Lahti, T. Suhonen, and J. Metsäjoki, "Dielectric Breakdown Strength of Thermally Sprayed Ceramic Coatings: Effects of Different Test Arrangements," J. Therm. Spray Technol., Vol. 24, No. 3, pp. 542–551, 2015.
[13] M. Niittymäki, T. Suhonen, J. Metsäjoki, and K. Lahti, "Electric Field Dependency of Dielectric Behavior of Thermally Sprayed Ceramic Coatings," IEEE 11th Int'l. Conf.e Properties and Applications of Dielectr. Materials (ICPADM), pp. 500–503, 2015.
[14] J. Kotlan, R. C. Seshadri, S. Sampath, P. Ctibor, Z. Pala, and R. Musalek, "On the dielectric strengths of atmospheric plasma sprayed Al_2O_3, Y_2O_3, ZrO_2–7% Y_2O_3 and $(Ba,Sr)TiO_3$ coatings," Ceram. Int., Vol. 41, No. 9, pp. 11169–11176, 2015.
[15] M. Niittymäki, T. Suhonen, J. Metsäjoki, and K. Lahti, "DC Dielectric Breakdown Behavior of Thermally Sprayed Ceramic Coatings," 24th Nordic Insul. Sympos. Materials, Components and Diagnostics, pp. 80–85, 2015.
[16] L. A. Dissado and J. C. Fothergill, *Electrical Degradation and Breakdown in Polymers*, First edit., The Institution of Electrical Engineering and Technology, London, UK, 1992.
[17] R. Bartinikas and R. M. Eichhorn, Eds., *Engineering Dielectrics* Vol. IIA, *Electrical Properties of Solid Insulating Materials: Molecular Structure and Electrical Behavior*. Philadelphia, USA: American Society for Testing and Materials, 1983.
[18] C. Neusel, H. Jelitto, and G. A. Schneider, "Electrical conduction mechanism in bulk ceramic insulators at high voltages until dielectric breakdown," J. Appl. Phys., Vol. 117, No. 15, p. 154902, 2015.
[19] F. Talbi, F. Lalam, and D. Malec, "DC conduction of Al_2O_3 under high electric field," J. Phys. D. Appl. Phys., Vol. 40, No. 12, pp. 3803–3806, 2007.
[20] "IEC standard 60093 Methods of test for volume resistivity and surface resistivity of solid electrical insulating materials," no. IEC Standard 60093. IEC, 1980.
[21] M. Lenzlinger, "Fowler-Nordheim Tunneling into Thermally Grown SiO_2," J. Appl. Phys., Vol. 40, No. 1, p. 278, 1969.
[22] J. J. O'Dwyer, *The Theory of Electrical Conduction and Breakdown in Solid Dielectrics*. Oxford: Clarendon Press, 1973.

Minna Niittymäki (S'13) was born in Sahalahti, Finland, on 29 March 1984. She received the M.Sc. degree in electrical engineering from Tampere University of Technology in 2012. Since then she has been working as Researcher in the high voltage research group of the Department of Electrical Engineering at TUT, with the aim towards Ph.D. degree. Her current research interests are in the area of insulation materials focusing on the dielectric characterization of thermally sprayed insulating ceramic coatings.

Kari Lahti (M'01) was born in Hämeenlinna, Finland in 1968. He received the M.Sc. and Doctoral degrees in electrical engineering from Tampere University of Technology in 1994 and 2003, respectively. Since then he has worked at the Department of Electrical Engineering at TUT, currently as a Research Manager and Adjunct Professor. He is the head of TUT's research group on high voltage insulation systems. He has also been responsible for the high voltage laboratory services at TUT since 2002. His research interests are in the area of high voltage engineering including surge arresters, nanocomposite insulation systems, environmental testing of high voltage materials and apparatus, high voltage testing methods and dielectric characterization of insulating materials.

Tomi Suhonen was born in Helsinki, Finland, on 24 December 1978. He is a Senior Scientist and Manager of multiscale materials modelling activities at VTT Technical Research Centre of Finland. He has 13 years' experience in scientific research related to advanced materials and has published more than 70 scientific papers and holds several international patents.

Jarkko Metsäjoki was born in Rauma, Finland, on 18 March 1982. He received M.Sc. degree in materials science from Tampere University of Technology (TUT) in 2008. He has worked at TUT, Braunschweig University of Technology, and since 2012 he has been working at VTT Technical Research Centre of Finland Ltd as Research Scientist. He is currently also a PhD student at Aalto University. His research interests include material characterization of thermally sprayed ceramic coatings.